RSC Advances

Accepted Manuscript

Journal Name

ARTICLE

Effect of nitrogen substitution on the structural and magnetic ordering transitions of $NiCr_2O_4$ †

Xin Liu,[a,b*] Nan Yin,[a] Tiju Thomas,[c] Minghui Yang,[a*] Junhu Wang[a,b] and Quan Shi[a*]

The nitrogen(N) doped spinel $NiCr_2O_4$ has been synthesized at 773 K (N500) and 873 K (N600) by ammonolysis of $NiCr_2O_4$ powders to study the effect of anion doping on its structural and magnetic properties. The N contents are determined by thermogravimetic oxidation, yielding a composition that can be described as $NiCr_2O_{3.68}N_{0.21}$ (N500) and $NiCr_2O_{3.55}N_{0.30}$ (N600). X-ray photoelectron spectroscopic studies suggest that N^{3-} species partly substitute the oxygen in the lattice and oxygen vacancies exist in the N doped samples. There is evidence that in the nitrided sample, Cr ion is most likely in a mixed oxidation state. As the N content increasess, the structure at room temperature changes from tetragonal to the cubic phase; N500 is only partially tetragonal; N600 is completely cubic. Such structural change is the consequence of the depression of the cooperative Jahn-Teller effect of Ni^{2+} in tetrahedral A site caused by the presence of N^{3-}. Combined heat capacity and the temperature dependent magnetic susceptibility measurements give clear evidence of the magnetic and structural transitions in the N doped $NiCr_2O_4$. The Jahn-Teller transition temperatures decrease with increasing N content; this is likely due to increased covalency and hence enhanced contribution of the angular momentum and the spin-orbit coupling to local chemical bonding around Ni^{2+}. Antiferromagnetic transitions are observed at Ts=23 K and 22K for N500 and N600, respectively. Hence there is indeed a lowering of transition when compared to pure $NiCr_2O_4$(28 K). The magnetic loops at different temperatures confirm that the material behaves as a paramagnet over a wide range of temperatures T~80-350 K. The material also exhibits a canted ferrimagnetic structural transition between 30 and 70 K. We also report evidence for increased frustration and lowered correlation length in N doped compounds compared to the parent $NiCr_2O_4$. The present study on N^- doping effects on the structure and magnetic properties of this $NiCr_2O_4$ is expected to be useful for tailoring the ferric phase transitions through anion substitutions.

1. Introduction

Nickel chromite ($NiCr_2O_4$) is a normal spinel and a common mineral in Earth's mantle and crust[1, 2]. It is commonly used for catalytic applications[3-6] and gas sensors[7]. It is also a well known magnetodielectric material that was first reported by Mufti et al[8]. The spinel $NiCr_2O_4$ exhibits interesting structural-magnetic correlation[9, 10]. In the cubic structure, Cr^{3+} (with $3d^3$ configuration) preferentially occupies the octahedral sites because of the strong crystal field stabilization of the half filled non-degenerate t_{2g} orbitals and empty e_g orbitals, while the

Ni^{2+} (with $3d^8$ configuration) are found in the tetrahedral sites[11]. The tetrahedral crystal field around Ni^{2+} ($3d^8$) in the cubic phase results in fully occupied low energy e levels and triply degenerate t_2 levels, rendering this structure potentially unstable. Consequently, a cooperative lattice distortion – from cubic to tetragonal symmetry - lifts the orbital degeneracy in $NiCr_2O_4$ at 310K[12]. This tetrahedral distortion results in the elongation of NiO_4 tetrahedra and c/a > 1. $NiCr_2O_4$ shows the occurrence of two magnetic transitions - T_C and T_S, corresponding to the onset of a ferrimagnetic (longitudinal) component and an antiferromagnetic (transverse) component[13]. By using neutron scattering, Ishibashi and Yasumi have confirmed a further structural distortion from tetragonal symmetry to orthorhombic symmetry at 65 K, which is correlated with the onset of ferrimagnetic ordering[14, 15]. At lower temperatures, the $NiCr_2O_4$ exhibits a canted magnetic structure in which the ferromagnetic component and the antiferromagnetic (AF) component forms is consistent with long-range order below T_S=31 K. A distortion within the

[a.] *Dalian Institute of Chemical Physics, Chinese Academy of Sciences, Dalian 116023, China.*
[b] *Mössbauer Effect Data center, Dalian Institute of Chemical Physics, Chinese Academy of Sciences, Dalian 116023, China.*
[c] *Department of Metallurgical and Materials Engineering, Indian Institute of Technology Madras, Chennai 600036, Tamil Nadu, India. E-mail: shiquan@dicp.ac.cn (Q.S), myang@dicp.ac.cn (M.Y), liuxin01@dicp.ac.cn (X.L)*
†Electronic Supplementary Information (ESI) available: [details of any supplementary information available should be included here]. See DOI: 10.1039/x0xx00000x

ARTICLE

orthorhombic structure takes place at the same temperature, where anomalies in magnetic susceptibility and heat capacity are found[16, 17]. The investigation of temperature and magnetic field dependence of dielectric properties reveals a new anomaly at 20 K, corresponding to the completion of structural and magnetic order[10].

Considering the rich structural chemistry of $NiCr_2O_4$ a lot of research efforts are ongoing to do with tailoring the phase transitions. Most of the work has been focused on modifications of cation composition, through doping of $Cu^{18, 19}$, Co^{20-22}, Mg^{23}, Fe^{24}, etc. into the $NiCr_2O_4$ lattice. In effect these studies explore the effect of the transition metal cations with different numbers of d electrons on observed structural distortions and the magnetic transition temperatures. A less explored approach is to investigate impact of anion composition on the structural transitions in $NiCr_2O_4$. Morris et al. reported that $NiCr_2S_4$ and $NiCr_2Se_4$ both have the Cr_3S_4 structure[25]. It is relevant to note that the Cr_3S_4(I2/m) system does not have a spinel structure, and that is is not antiferromagnetically ordered at low temperatures. In fact in this system, the order moments are reduced from spin only values, due to the appreciable covalency of the metal-sulfur bonds[26]. Hence the impacts of anion doping in an oxide material such as $NiCr_2O_4$ is certainly interesting.

Transition-metal oxides can be transformed into oxynitrides by reacting with ammonia at elevated temperatures. From the structural point of view, oxynitrides often show the same structural type as the parent oxides for moderate substitutional rates. Furthermore partial replacement of oxygen with nitrogen is readily obtained via ammonolysis[27-29]. The anionic substitution of divalent oxygen for trivalent nitrogen additionally induces a change in the oxidation state of the transition metals involved. This oftentimes yields insulating materials as a consequence of strong perturbation of the periodic potential at the anion substructure and due to the increased covalency in the materials since N is less electronegative than O^{30}.

A number of theoretical and experimental studies have focused on the electronic properties and electronic band gaps of the oxynitrides with spinel structure. Several studies have been carried out regarding ternary nitrides and oxynitrides[31] in an effort to tailor the desirable mechanical and electronic properties associated with spinel oxynitrides. Research has expanded further into spinel-type oxynitrides in an effort to engineer the band gap value by varying the N:O ratio. However, the highly reducing atmosphere during thermal ammonolysis hardly permits middle-to-late transition metals to form oxynitrides without being reduced to elemental metals or metal nitrides. For this reason, the highest content of nitrogen reported in materials with spinel crystal structures is rather low.

In this study, we first doped N in the lattice of $NiCr_2O_4$ spinel by ammonolysis of the precursor oxides under favourable conditions. Subsequently we employed X-ray powder diffraction (XRD), magnetic susceptibility, X-ray photoelectron spectra (XPS) and heat capacity (C_v) measurements to investigate the structural and magnetic transitions in N doped

$NiCr_2O_4$. We find this spinel exhibiting interesting physical properties: the Jahn-Teller (JT) distortion temperature decreases with increasing N concentration. In addition, the magnetic structure and magnetic interaction are also affected by the N doping.

2. Experimental details

Materials

$NiCr_2O_4$ is prepared by a solid state reaction of a stoichiometric mixture of powders of NiO (99.99%, Aldrich) and Cr_2O_3 (99.99%, Aldrich). The powders are ground together and heated for 24 h in air at a temperature of 1473 K with intermediate regrindings. 0.2 – 0.3 g of these samples are placed in an alumina boat. The boat is then placed in a silica tube which has air tight stainless steel end caps; these caps have welded valves and connections to input and output gas lines. All gases used are purified to remove trace amounts of oxygen or water using pellet copper, nickel, palladium and platinum with zeolites as support. The silica tube is then placed in a split tube furnace and the appropriate connections to gas sources are made. Argon gas is passed over the sample for 15 min to expel air before establishing a flow of ammonia gas (anhydrous, Air Gas). The $NiCr_2O_4$ is heated at the reaction conditions as summarized in Table 1. After treatment for the specified period, the furnace power is turned off and the product is cooled to room temperature for ~ 4 h under ammonia flow conditions. Before the silica tube is taken out of the split tube furnace, argon gas is flowed through the silica tube to expel the ammonia gas. The samples treated at 773 K and 873 K are represented as N500 and N600, respectively.

Characterization

Finely ground powders are examined with a Rigaku Ultima VI powder X-ray diffractometer (PXRD) with monochromatic $CuK_{\alpha 1}$ radiation (λ = 1.5406 Å). Crystal structures of the oxide and the resulting nitride are confirmed by PXRD profiles using the GSAS package. Scanning electron microscopy (SEM) is performed with a LEO-1550 field emission SEM (FSEM). The dc-magnetic susceptibility is measured with a Physical Property Measurement System (PPMS) over the 4-350 K temperature range. Magnetization isotherms are measured at selected temperatures in the magnetic field range from -4T to +4T. Thermal gravimetric analyses (TGA) are performed with a SETSYS 16/18 (SETARAM) in a temperature range of 300 - 1273 K. The heat capacity measurement is performed using a Physical Property Measurement System (PPMS) in the temperature range from (1.9 to 400) K, and the measurement uncertainties are verified to be ±3% below 20 K and ±1% from (20 to 400) K.[32] The detailed heat capacity measurement procedure can be found in the related work reported by Shi *et al.* [32, 33]. The binding energy of the surface Ni, Cr, O, N species are determined by X-ray photoelectron spectra (XPS) with an ESCALAB250 X-ray photoelectron spectrometer using contaminated C as internal standard (C1s=284.6 eV)

Journal Name ARTICLE
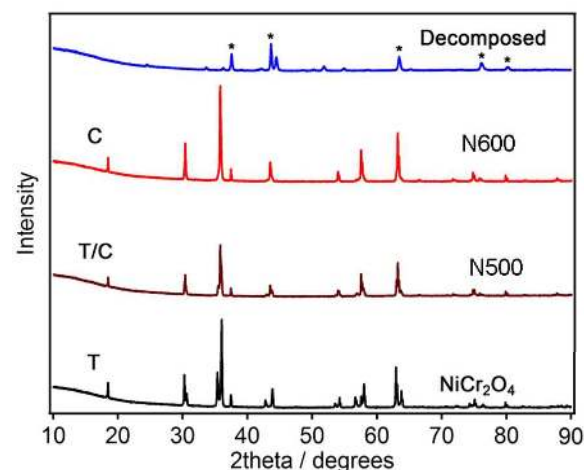
Results and discussion

Fig. 1 PXRD patterns for $NiCr_2O_4$: N500 and N600. T stands for tetrahedral phase and C stands for cubic phase of $NiCr_2O_4$. * stands for CrN.

The XRD patterns for the $NiCr_2O_4$ and the ammonolyzed products can be seen in fig. 1. The X-ray diffraction profile is fitted to confirm the phase purity of the $NiCr_2O_4$ products as shown in Figure S1. The as prepared $NiCr_2O_4$ has a tetragonal structure in space group I41/amdz with refined lattice parameters a=5.8319(2) Å and c=8.4433(2) Å (ref: Table 1). The ammonolysis product of $NiCr_2O_4$ at 873 K has a cubic structure in the space group Fd-3mz with lattice parameters a = 8.3181(2) Å. The ammonolysis product of $NiCr_2O_4$ at 773 K is a mixture of two phases, containing mainly cubic phase. Presence of tetragonal $NiCr_2O_4$ in N500 is indicated by the small shoulder peak at ~37 degrees in PXRD pattern. The slightly larger lattice parameters and volume for the oxynitride is due to the ionic radius of N^{3-} (1.46Å) being greater than the ionic radius of O^{2-}(1.38 Å)[34]. Ammonolysis treatment of the $NiCr_2O_4$ at higher temperature (>873 K) results in decomposition to $NiCrO_3$ and CrN. Both as-prepared and ammonolysis products of $NiCr_2O_4$ have similar average crystalline domain sizes of ~76 nm, calculated from PXRD refinements. These results agreed well with results obtained from electron micrography. The precise location of the nitrogen atoms of the oxynitrides cannot be obtained by XRD due to the similar X-ray scattering factors of N^{3-} and O^{2-}. Hence measurement of neutron diffraction is needed; this will be pursued in future.

SEM images are used to observe the surface morphology of the products given in Figure S2. This figure confirms that the powder sample is contains large particle of size ~70-400 nm. The ammonolyzed samples are designated as $NiCr_2O_{4-x}N_{2x/3}$. The nitrogen contents are analyzed by converting $NiCr_2O_{4-x}N_{2x/3}$ back to $NiCr_2O_4$ using TG in air flow as shown in Figure S3. The calculated average compositions are $NiCr_2O_{3.68}N_{0.21}$ and

$NiCr_2O_{3.55}N_{0.30}$ for products ammonolysed at 773 and 873 K, respectively.

Table 1: Refined lattice parameters and calculated domain size of $NiCr_2O_4$ and its ammonolysis products.

Formula	$NiCr_2O_4$	$NiCr_2O_{3.68}N_{0.21}$	$NiCr_2O_{3.55}N_{0.30}$
Formula weight	226.68	224.50	223.69
Crystal system	Tetrahedral	Cubic	Cubic
Space group	I41/amd	Fd-3m	Fd-3m
a/Å	5.8319(1)	8.3181(2)	8.3184(1)
c/Å	8.4433(1)	-	-
V/ Å³	287.17(1)	575.53(1)	575.60(1)
ρ_{calcd}/kg m⁻³	5.243	5.232	5.232
$_wR_p$	0.0462	0.0455	0.0410
R_p	0.0274	0.0263	0.0249
Domain size$_{Calcd}$	77	78	66

Fig. 2 (a-d) presents the O 1s, N 1s, Cr 2p and Ni 2p core level X-ray photoelectron spectra(XPS) of N500 respectively. Each spectrum is fitted by a least squares method using Gaussian-Lorentzian envelopes. The surface stoichiometry of the sample calculated from the XPS data is N(3.73%), O(64.86%), Ni(10.98%), Cr(20.43%). As seen, the surface stoichiometry of the sample is close to the bulk of the sample; surface oxygen concentration however is quite different. The O 1s spectra are fitted with an O^{2-} component at 529.9eV along with additional peaks with binding energy (BE) at 530.9 eV and 531.9 eV. The most prominent peak at 529.9 eV corresponds to the lattice O^{2-}, while the peak at 530.9 eV is assigned to the defect states within the crystal.[35-38] The additional peak at 531.9 eV is associated with the O present in Cr-N-O or Ni-N-O bonds.[39]

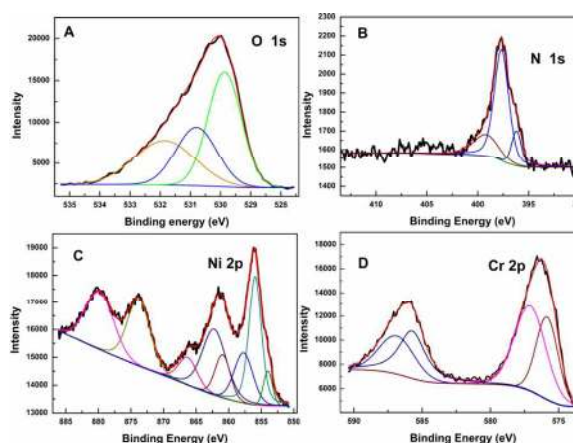Fig. 2 The O 1s (A), N 1s (B), Ni 2p (C) and Cr 2p(D) XPS spectra for N500.

ARTICLE   **Journal Name**

In Figure 2(a), the N 1s features show only one asymmetric peak with a binding energy (BE) of 395-402 eV. On deconvolution, it can be seen that the broad peak consists of three different peaks at ~396.2, 397.7 and 399.2 eV respectively. The main peak with the binding energies of 397.7 eV is assigned to Cr-N or Ni-N species[40, 41]; this suggests that nitrogen substitutes for oxygen in the spinel matrix. The peak with binding energy at ~396.2 eV is indicative of a N^{3-} species[42, 43] and confirms the presence of oxynitride species with lower binding energy[44]. Interestingly the BE observed here for N^{3-} is lower than that for NiN[45] or CrN(396.3 - 397.1 eV)[46, 47]; this suggests greater charge transfer to the nitrogen in $NiCr_2O_4$, when compared to the pure nitrides. However there could be a contribution from oxygen vacancy formation induced by N doping as well[48]. The peak at 399.2eV is attributed to nitrogen in the interstitial sites, where nitrogen has mixed Cr-O-N or O-Cr-N (Ni-O-N, O-Ni-N) environment. In this state, N atoms are bonded to one or more lattice oxygen ions[47, 49] and therefore are in a relatively positive oxidation state[50]. From literature, [18, 21] the values of BE for the Ni 2p level and of the satellite shift ΔE permit identification of the Ni ions; they are divalent in tetrahedral environments. The Cr 2p spectra of the sample has a multiplet shape that is typical for Cr^{3+} ions[51]. The incorporation of nitrogen into lattice results in Cr-N or Ni-N bonds, which is supported by the lower BE of Ni 2p and Cr 2p in N doped $NiCr_2O_4$. Marginal decrease in BE of Cr and Ni are reasonable since addition of N reduces the overall ionic character of the compounds, increasing the electron density around cations. Hence, in Fig. 2 (c) and (d), the negative shifts are observed in Cr 2p and Ni 2p binding energies. The peak of Cr 2p is close to 576.0 eV which corresponds to Cr^{2+}. Hence it is difficult to prove the existence of Cr^{2+} ions because of the small difference between the obtained value of binding energy and that of Cr^{2+}. Therefore it is very likely that Cr ions exist in mixed oxidation states (i.e 3^+ as well as 2^+) in N doped $NiCr_2O_4$.

To investigate the magnetic and structural evolution of the $NiCr_2O_4$ samples during the ammonolysis process in thermodynamics, the heat capacities of the $NiCr_2O_4$ and N doped samples are measured using the PPMS in the temperature range from (1.9 to 400) K. The experimental heat capacities are plotted against the temperature and compared with the reported values from Klemme et al[17] (Fig. 3). It can be seen from the figure that the heat capacity of the as-prepared $NiCr_2O_4$ are in agreement with published values revealing three thermal anomalies at around 310 K, 66 K and 29 K, respectively. Based on the previous magnetic and structure studies[13], the thermal anomaly appearing at 310 K (the first transition) has been attributed to a cooperative Jahn-Teller distortion lifting the orbital degeneracy in $NiCr_2O_4$, resulting in a structural transition from cubic to tetragonal. The other two anomalies at 66 K (the second transition) and 29 K (the third transition) have been accounted for by a longitudinal and a transverse antiferromagnetic ordering, respectively. As for the nitride samples; with increase in N content, the first and third transitions move to lower temperatures, while the second one moves to higher temperatures. The lattice heat capacities of these samples have been estimated by fitting the experimental
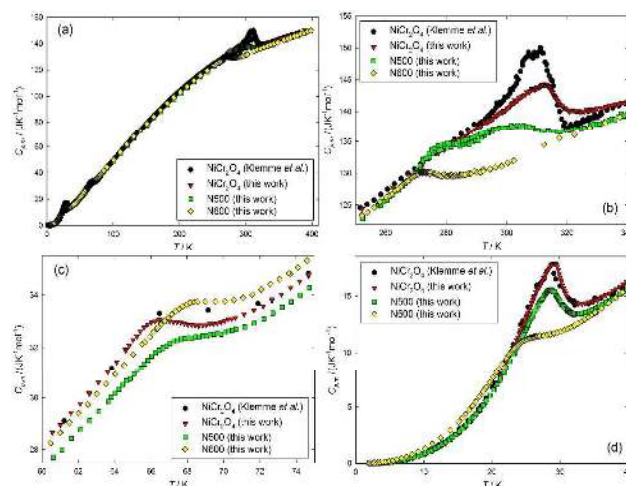

Fig. 3 Plot of heat capacities of $NiCr_2O_4$ (measured by Klemme *et al.*[17] and in this work), N500 and N600 as a function of temperature over the temperature ranges: (a) from (1.9 to 400) K, (b) from (250 to 340) K, (c) from (60 to 75) and (d) from (1.9 to 40).

heat capacities in the corresponding temperature windows to a combination of Debye and Einstein functions, and the fitting equation can be expressed by

$$C_{p,m}=m \cdot D(\Theta_D/T)+n_1 \cdot E(\Theta_{E,1}/T)+n_2 \cdot E(\Theta_{E,2}/T) \qquad (1)$$

where $D(\Theta_D/T)$, $E(\Theta_{E,1}/T)$ and $E(\Theta_{E,2}/T)$ are Debye, low and high temperature Einstein functions, respectively. m, n_1, n_2, Θ_D, $\Theta_{E,1}$ and $\Theta_{E,2}$ are adjustable parameters; the sum of $(m + n_1 + n_2)$ is approximately equal to the number of atoms in the molecule[52-54]. The fitting parameters from Eq. (1) are listed in Table S1. The heat excess heat capacities due to the three transitions have been calculated by subtracting the estimated lattice heat capacities from the total, and the results are shown in Figure S4. Consequently, the starting, ending and peak temperatures and the entropy changes related to the three transitions have been determined in Table S2 based on the excess heat capacities.

As can be seen from Figure S4(a), the peak temperature of the first transition moves to the lower temperatures with increase in N concentration. Also, the transition entropy decreases from 1.14 $J \cdot K^{-1} mol^{-1}$ to 0.59 $J \cdot K^{-1} mol^{-1}$ as the N anions concentration increases from $NiCr_2O_4$ to N600. This indicates that the Jahn-Teller distortion effect on the structural transition has been suppressed in these samples. The second transition due to the paramagnetic to ferrimagnetic ordering only has a slight influence on transition temperatures and entropies, suggesting that the doped N hardly affects the magnetic ordering. However, as for the third transition related to the antiferromagnetic ordering, the peak temperature moves from 29 K to 24.3 K, and the transition entropy changes

to almost half the amount, decreasing from 2.53 J·K^{-1}mol^{-1} to 1.30 J·K^{-1}mol^{-1}. This suggests that the doped N is likely to produce a significant effect on the thermodynamic behaviour of the third transition.

The heat capacity of a substance can be generally expressed as a sum of contributions from various modes related to the lattice, electronic, magnetic and others. Each of these contributions may be fitted to the corresponding theoretical models which would help in elucidation of important information about the physical properties of the substance[55]. The lattice heat capacity far outweighs all other contributions at high temperature regions (above 15-20 K). However, at low temperatures (below 15-20 K) the lattice is comparable to the other contributions, and therefore each of these contributions can be extracted by fitting the total heat capacity to theoretical models in carefully chosen temperature regions. In order to further understand the observed specific heat capacity trends measured for NiCr$_2$O$_4$ and N-doped samples, the experimental heat capacities of these compounds below 10 K have been fitted to a theoretical function of:

$$C_{p,m} = \gamma T + B_3 T^3 + B_5 T^5 + B_7 T^7 + B_{asw} T^3 e^{-\Delta/T} \qquad (2)$$

Here the linear term is usually a contribution from electrons as well as vacancies or dislocations existing in the samples. The odd-powers in temperature represent the lattice vibration contribution. As for the magnetic contribution, it is represented using the term $B_{asw} T^3 e^{-\Delta/T}$, where B_{asw} is defined as the antiferromagnetic constant proportional to molar volume and the spin-wave stiffness constant. Δ is the magnetic spin-wave gap written in Kelvins[52-54]. The antiferromagnetic contribution decreases in the N-doped samples, implying that the magnetic ordering is likely reduced to some extent as the nitrogen atoms get implanted in the lattice. Moreover the linear term tends to increase as we go from NiCr$_2$O$_4$ to N600, suggesting that the increasing nitrogen doping does result in increasing vacancy concentrations. The values relevant to the specific heat capacity measurements are listed in Table S3. It can be seen from the results that the antiferromagnetic contribution does exist in the heat capacities. This further confirms the presence of antiferromagnetic ordering.

Fig. 4(a-c) shows the temperature dependence of susceptibility in NiCr$_2$O$_4$ and N doped samples, as measured after field cooling; a magnetic fields up to 1000 Oe is applied for getting the data. The observed magnetic data is analyzed using the equation given below below:

$$\chi = \chi_0 + \frac{C}{T - \Theta_{cw}} \qquad (3)$$

Where C is the Curie constant, Θ_{CW} is the Curie Weiss temperature and χ_0 is a temperature-independent Pauli-like term. In Figure 4(a), as the temperature decreases, there is a small kink at 315 K in the inverse susceptibility curve, corresponding to the cooperative Jahn-Teller (J-T) transition An abrupt rise in the susceptibility curve at T$_C$=66 K

corresponds to the ferrimagnetic transition. Further change in magnetic structure occurs at T$_S$=28 K, where another anomaly
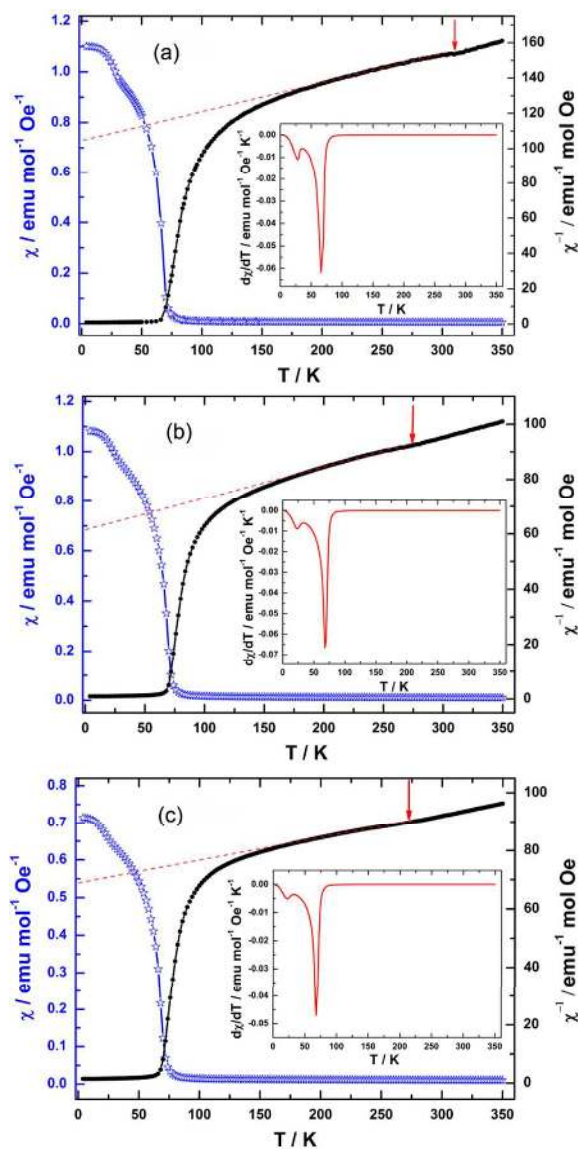

Fig. 4 The temperature dependence of susceptibility (Blue) and inverse susceptibility curves (Black) for NiCr$_2$O$_4$(a), N500(b) and N600(c). The arrows indicate the J-T transitions. The insets are the related temperature derivative of the susceptibilities, and the peaks corresponding to the T_C and T_S respectively

in this curve is observed. These structural and magnetic transition temperatures are in good agreement with other reports for polycrystalline NiCr$_2$O$_4$[14, 56].

For the N doped samples, the J-T distortions occur at 275 K (N500) and 268 K (N600) respectively, which become lower than the transition temperature of pure NiCr$_2$O$_4$. The ferrimagnetic ordering (T_C) occurs at 67 and 68 K, which is a

ARTICLE

minor increase after the N doping. In contrast to ferrimagnetic transition, the antiferromagnetic (transverse) ordering transition (T_S) is decreasing from 28 K to 22 K with N doping. These transition temperatures corroborate well with the heat capacities results. When N atoms replace O atoms, the N ions would provide empty 2p orbitals for the formation of covalent bonds with Ni^{2+} and Cr^{3+} [57]. This likely causes a reduction of the J-T potential energy; the driving force for the J-T distortion would hence be reduced[58, 59]. The decreasing of distortion would enhance the contribution of the angular momentum and the spin-orbit coupling, and as a result, J-T transition temperature would further fall off[60]. This in turn would stabilizes the cubic structure and leads to the gradual decrease in the tetragonal distortion temperature.

The Curie Weiss (CW) equation (3) is applied to fit the paramagnetic regimes of the susceptibility before the onset of the J-T distortion for the $NiCr_2O_4$ and N doped samples. The obtained effective moments (μ_{eff}) and CW temperatures are listed in Table S4. The experimental value of μ_{eff} is 6.43 μ_B for $NiCr_2O_4$, which is slightly larger than the expected 6.16 μ_B per formula unit[16]. Hence we infer that although the angular momentum is largely quenched due to the tetragonal distortion, there is still a small contribution of the partially quenched orbital moments of Ni ions to the overall magnetic moment per formula unit. For the N doped $NiCr_2O_4$, the temperature independent Pauli term χ_0 increases due to the covalent effect. The effective moments increase with increasing N content from 7.64 μ_B to 8.04 μ_B. This further corroborates the hypothesis that unquenched orbital moments of Ni^{2+} in the tetrahedral sites of the cubic structure make an important contribution to the magnetic moment[61]. Magnetic contributions may also come from the impurity/dopant atoms[62], as well as the oxygen vacancies[63].

The CW temperature of $NiCr_2O_4$ is -489 K，while N600 present even larger CW temperatures of -594 K. The exchange coupling between magnetic ions (Ni^{2+} and Cr^{3+}) is directly proportional to CW temperature and can be expressed as:

$$J = A|\Theta_{CW}| \qquad (4)$$

Where $A=3k_B/ZS(S+1)$, k_B is the Boltzmann constant, Z is the number of the interactions of nearest neighbours, and S is the total spin. The negative value of Θ_{CW} indicates the presence of antiferromagnetic or ferrimagnetic correlation interaction, while the magnitude of Θ_{CW} for the oxynitrides suggests that the antiferromagnetic interaction is enhanced. The orbits of tetrahedral Ni^{2+} ions and octahedral Cr^{3+} can be characterized by $e^4t_2^4$ and $t_{2g}^3e_g^1$ electronic configurations respectively. It is known that the Cr^{3+} ion, in octahedral site with empty e_g orbits antiferromagnetically interact with Ni^{2+} in tetrahedral site, [64] In fact, calculation suggests that the direct Cr-Cr exchange constant (J_{Cr-Cr}) could be over three times larger than the superexchange Cr-O-Ni interaction constant[65]. In the $NiCr_2O_4$ chromite, increase in CW suggests stronger B-B direct exchange interaction among magnetic ions, which increases

with N doping level. Furthermore, the frustration index (Θ_{CW}/T_N) of N600 is 8.74, indicating that N doped samples are the more frustrated compounds compared to the parent $NiCr_2O_4$.

It should also be mentioned that the deviation of the reverse susceptibility against T curve from a straight line begins below a temperature of 176 K, 160K, and 152 K respectively. The deviation observeed is a slow downward drop. This downward deviation from the Curie-Weiss law indicates the onset of a magnetic short-range interaction just above T_C. The decrease of deviation temperature means that N doping produces a decrease in correlation length.
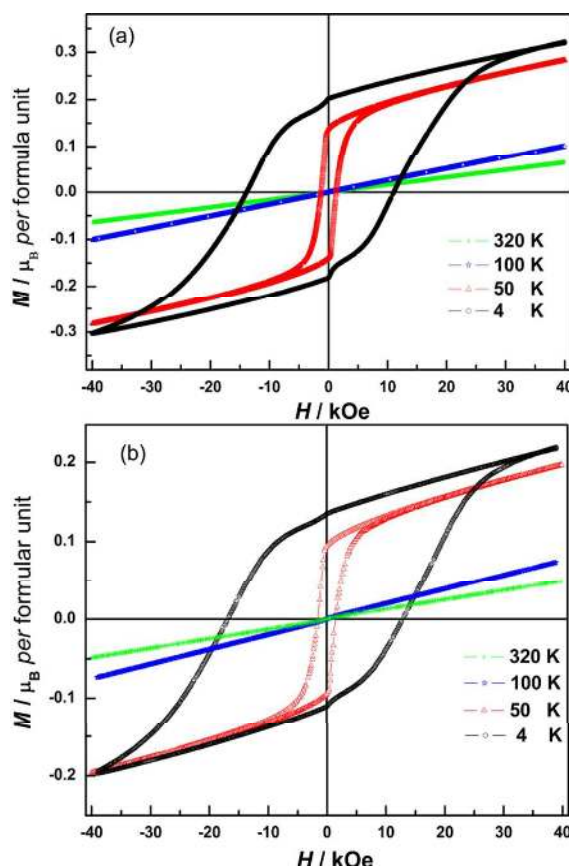

Fig. 5 Isothermal field-dependent magnetization of N500 (a) and N600 (b) measured at 4 K, 50 K, 100 K and 320 K respectively

To gain further insight into the magnetic properties of the synthesized N doped $NiCr_2O_4$ samples, magnetization (M) as a function of applied magnetic field (H) is measured at different temperatures (Figure 5). For N500 and N600, the magnetization linearly increases with field while measured at 320 K and 100 K, and there is no magnetic hysteresis and hence the remanence (M_r) and coercivity (H_C) are practically zero. This indicates a paramagnetic behavior. This is consistent with the M-T plots in Figure 4. However, very clear magnetic

Please do not adjust margins

RSC Advances

Journal Name

ARTICLE

Table II: The magnetic parameters of $NiCr_2O_4$, N500 and N600

Sample	C (emu*K/mol)	θ_{CW} (K)	M_{eff} (μ_B)	χ_0 (emu /mol*Oe)	T_S (K)	T_N (K)	M_S (μ_B)	H_C (Oe)
$NiCr_2O_4$	5.18	-486	6.43	0.00008	28	66	0.30[]	8300[]
N500	7.30	-456	7.64	0.00084	23	67	0.30	12500
N600	8.08	-594	8.04	0.00188	22	68	0.28	15000

hysteresis loops appear at 50 K with H_C, M_r and spontaneous magnetization (M_s) values listed in Table II. The area under hysteresis increases with significant increase in coercivity (H_c). We observe higher H_C of 14 kOe for N600 compared with 8.3 kOe for $NiCr_2O_4$[10]. The larger coercive field indicates presence of ferromagnetic long-range order and stronger magnetic anisotropy which may be caused by the spin-orbit interaction. At 50 K, the magnetization readily increases at low field and then linearly increases up to 40 kOe without showing any saturation for both N doped samples.

When temperature goes down to 4 K, the isotherm M(H) still did not exhibit saturation, and the spontaneous magnetization of N doped $NiCr_2O_4$ is estimated to be 0.2 μ_B per formula unit. Considering the fact that H_C is found to be less than 15 kOe, we suggest that this linear contribution signals a non-collinear spins arrangement of the $NiCr_2O_4$ ferrimagnet. As is stated in references[66, 67], in non-collinear configuration the applied magnetic field exerts a torque that could change the angles between the canted magnetic moments. Hence the magnetization is expected to increase linearly with the magnetic field in this temperature regime. Since the magnetic moment of the tetrahedral sublattices in $NiCr_2O_4$ is greater in magnitude than that of the octahedral sublattice $(M_A>M_B)$[68], and the magnetic structure consists of longitudinal and transverse magnetic sublattices with slight canting of spins[13]. This suggests that when N is incorporated in the lattice, crystalline anisotropy and magnetostrictive effects associated with spin-orbit coupling have increased the noncollinearity of tetrahedral sbulattice spins. This decreases the noncollinearity of octahedral sublattices[68]. Hence the magnetic ordering in $NiCr_2O_4$ and the N doped samples is strongly coupled to structure. Further investigations are required to obtain greater clarity regarding correlations between magnetic and structural changes in this interesting material.

The N doped $NiCr_2O_4$ has been synthesized successfully by nitridation of the solid $NiCr_2O_4$ oxides at 773 K(N500) and 873 K (N600) respectively. The incorporation of N into the lattice has been confirmed using XRD and XPS measurements. The susceptibility and heat capacity based investigations indicate that structural and magnetic properties undergo significant changes upon N doping. Pure $NiCr_2O_4$ exists in tetragonal structure, however N500 and N600 contains cubic phase at room temperature. The temperature of cooperative Jahn-Teller distortion decreases with increase in N content. This observation is related to change in nature of bonding brought about by introduction on N into the lattice. The ferrimagnetic ordering temperature (T_C) of the material exhibits a minor increase indicating that the A-B superexchange interaction is not affected much by the N-doping due to the empty e_g orbital of Cr ions (which is present in the octahedral site). The N doped $NiCr_2O_4$ exhibits a canted ferrimagnetic structural transition between 30 and 70 K. We also report evidence for increased frustration and lowered correlation length with N doping in $NiCr_2O_4$. The hitherto unexplored details of magnetostructural coupling are likely to stimulate further investigations on this interesting material.

Acknowledgements

Conclusions

ARTICLE

Journal Name

References

1. A. E. Ringwood, *McGraw-Hill International Series in the Earth and Planetary Sciences: Composition and Petrology of the Earth's Mantle*, 1975.
2. F. C. Romeijn, *Philips Research Reports*, 1953, **8**, 304-320.
3. N. J. Jebarathinam, M. Eswaramoorthy and V. Krishnasamy, *Bull. Chem. Soc. Jpn.*, 1994, **67**, 3334.
4. G. Vivekanandan and V. Krishnasamy, *Hung. J. Ind. Chem.*, 1995, **23**, 21.
5. J. Sloczynski, J. Ziolkowski, B. Grzybowska, R. Grabowski, D. Jachewicz, K. Wcislo and L. Gengembre, *J. Catal.*, 1999, **187**, 410.
6. B. L. Dubey, N. B. Singh, J. N. Srivastava and A. K. Ojha, *Indian J. Chem., Sect. A: Inorg., Bio-inorg., Phys., Theor. & Anal. Chem.*, 2001, **40A**, 841.
7. C. L. Honeybourne and R. K. Rasheed, *J. Mater. Chem.*, 1996, **6**, 277.
8. N. Mufti, A. A. Nugroho, G. R. Blake and T. T. M. Palstra, *J. phys. Condens. matter.*, 2010, **22**, 075902.
9. C. O. Augustion, D. Prabhakaran and L. K. Srinivasan, *J. Mater. Sci. Lett.*, 1993, **12**, 383.
10. T. D. Sparks, M. C. Kemei, P. T. Barton, R. Seshadri, E.-D. Mun and V. S. Zapf, *Phys. Rev. B: Condens. Matter Mater Phys.*, 2014, **89**, 024405.
11. J. D. Dunitz and L. E. Orgel, *J. Phys. Chem. Solids*, 1957, **3**, 20.
12. G. Ueno, S. Sato and Y. Kino, *Acta Crystallogr., Sect. C: Cryst. Struct. Commun.*, 1999, **C55**, 1963.
13. K. Tomiyasu and I. Kagomiya, *J. Phys. Soc. Jpn.*, 2004, **73**, 2539.
14. E. Prince, *J. Appl. Phys.*, 1961, **32**, 68.
15. H. Ishibashi and T. Yasumi, *J. Magn. Magn. Mater.*, 2007, **310**, e610.
16. M. R. Suchomel, D. P. Shoemaker, L. Ribaud, M. C. Kemei and R. Seshadri, *Phys. Rev. B: Condens. Matter Mater. Phys.*, 2012, **86**, 054406.
17. S. Klemme and J. C. van Miltenburg, *Phys. Chem. Miner.*, 2002, **29**, 663.
18. M. Lenglet, A. D'Huysser, J. Arsene, J. P. Bonnelle and C. K. Joergensen, *J. Phys. C: Solid State Phys.*, 1986, **19**, L363.
19. M. Tovar, R. Torabi, C. Welker and F. Fleischer, *Phys. B*, 2006, **385-386**, 196.
20. A. S. Mikheykin, D. Y. Chernyshov, A. A. Bush, A. S. Prokhorov, Y. I. Yuzyuk and V. P. Dmitriev, *Phys. Solid State*, 2014, **56**, 785.
21. A. G. Kochur, A. T. Kozakov, K. A. Googlev, A. S. Mikheykin, V. I. Torgashev, A. A. Bush and A. V. Nikolskii, *J. Electron Spectrosc. Rela. Phenom.*, 2014, **195**, 208.
22. M. Ptak, M. Maczka, A. Pikul, P. E. Tomaszewski and J. Hanuza, *J. Solid State Chem.*, 2014, **212**, 218.
23. B. D. Hosterman, J. W. Farley and A. L. Johnson, *J. Phys. Chem. Solids*, 2013, **74**, 985.
24. L. G. Antoshina, A. N. Goryaga and D. A. Chursin, *Phys. Solid State*, 2002, **44**, 747.
25. B. L. Morris, P. Russo and A. Wold, *J. Phys. Chem. Solids*, 1970, **31**, 635.
26. A. V. Powell, D. C. Colgan and C. Ritter, *J. Solid State Chem.*, 1997, **134**, 110.
27. M. J. Martinez-Lope, M. T. Casais and J. A. Alonso, *Z.Naturforsch.(B)*, 2006, **61**, 164.
28. M. T. Weller and S. J. Skinner, *Int. J. Inorg. Mater.*, 2000, **2**, 463.
29. M. Retuerto, C. de la Calle, M. J. Martinez-Lope, F. Porcher, K. Krezhov, N. Menendez and J. A. Alonso, *J. Solid State Chem.*, 2012, **185**, 18.
30. G. M. Veith, M. Greenblatt, M. Croft and J. B. Goodenough, *Mater. Res. Bull.*, 2001, **36**, 1521.
31. T. D. Boyko, C. E. Zvoriste, I. Kinski, R. Riedel, S. Hering, H. Huppertz and A. Moewes, *Phys. Rev. B: Condens Matter Mater. Phys.*, 2011, **84**, 085203.
32. R. Dai, S. Zhang, N. Yin, Z.-C. Tan and Q. Shi, *J. Chem. Thermodyn.*, 2016, **92**, 60.
33. Q. Shi, C. L. Snow, J. Boerio-Goates and B. F. Woodfield, *J. Chem. Thermodyn.*, 2010, **42**, 1107.
34. R. D. Shannon, *Acta Crystallogr., Sect. A:* 1976, **A32**, 751.
35. H. A. E. Hagelin-Weaver, J. F. Weaver, G. B. Hoflund and G. N. Salaita, *J. Electron Spectrosc. Relat. Phenom.*, 2004, **134**, 139.
36. P. R. Norton, R. L. Tapping and J. W. Goodale, *Surf. Sci.*, 1977, **65**, 13.
37. B. P. Payne, M. C. Biesinger and N. S. McIntyre, *J Electron Spectrosc. Relat. Phenom.* 2012, **185**, 159.
38. M. C. Biesinger, B. P. Payne, A. P. Grosvenor, L. W. M. Lau, A. R. Gerson and R. S. Smart, *Appl. Surf. Sci.*, 2011, **257**, 2717.
39. X. B. Chen and C. Burda, *J. Phys. Chem. B*, 2004, **108**, 15446.
40. S. Agouram, F. Bodart and G. Terwagne, *J. Electron Spectrosc. Relat. Phenom.*, 2004, **134**, 173.
41. I. Milosev, H. H. Strehblow and B. Navinsek, *Surf. Coat. Technol.*, 1995, **74-75**, 897.
42. M. Batzill, E. H. Morales and U. Diebold, *Phys. Rev. Lett.*, 2006, **96**.
43. S. Q. Xiao and O. Takai, *Thin Solid Films*, 1998, **317**, 137.
44. I. Milosev, J. M. Abels, H. H. Strehblow, B. Navinsek and M. Metikos-Hukovic, *J. Vac. Sci. Technol., A:* 1996, **14**, 2527.
45. G. Soto, W. de la Cruz and M. H. Farias, *J. Electron Spectros. Relat. Phenom.*, 2004, **135**, 27.
46. C. Palacio, A. Arranz and D. Diaz, *Thin Solid Films*, 2006, **513**, 175.
47. B. Subramanian and M. Jayachandran, *Corros. Eng. Sci. Technol.*, 2011, **46**, 554.
48. S.-H. Lee, E. Yamasue, K. N. Ishihara and H. Okumura, *Appl. Catal. B-Environ.,* 2010, **93**, 217.
49. Y. Cong, J. Zhang, F. Chen and M. Anpo, *J. Phys. Chem. C*, 2007, **111**, 6976.
50. R. A. R. Monteiro, S. M. Miranda, V. J. P. Vilar, L. M. Pastrana-Martinez, P. B. Tavares, R. A. R. Boaventura, J. L. Faria, E. Pinto and A. M. T. Silva, *Appl. Catal. B-Environ.*, 2015, **162**, 66.
51. M. C. Biesinger, C. Brown, J. R. Mycroft, R. D. Davidson and N. S. McIntyre, *Surf. Interface Anal.*, 2004, **36**, 1550.
52. Q. Shi, L. Zhang, M. E. Schlesinger, J. Boerio-Goates and B. F. Woodfield, *J. Chem. Thermodyn.*, 2013, **62**, 35.
53. Q. Shi, L. Y. Zhang, M. E. Schlesinger, J. Boerio-Goates and B. F. Woodfield, *J. Chem. Thermodyn.*, 2013, **62**, 86.
54. Q. Shi, L. Y. Zhang, M. E. Schlesinger, J. Boerio-Goates and B. F. Woodfield, *J. Chem. Thermodyn.*, 2013, **61**, 51.
55. E. S. R. Gopal, *Specific heats at low temperatures*, *The International Cryogenics Monograph Series*, 1966.
56. O. Crottaz, F. Kubel and H. Schmid, *J. Mater. Chem.*, 1997, **7**, 143.

57. M. H. Whangbo, H. J. Koo, A. Villesuzanne and M. Pouchard, *Inorg. Chem.*, 2002, **41**, 1920.
58. J. B. Goodenough and A. L. Loeb, *Phys. Rev.*, 1955, **98**, 391.
59. L. Cianchi, M. Mancini and P. Moretti, *Phys. Rev. B: Solid State*, 1973, **7**, 5014.
60. J. B. Goodenough, *Magnetism and the chemical bond*. 1963.
61. J. S. Smart, *Phys Rev*, 1954, **94**, 847.
62. A. Stashans and S. Jacome, *Comput. Mater. Sci.*, 2014, **81**, 353.
63. A. Sundaresan, R. Bhargavi, N. Rangarajan, U. Siddesh and C. N. R. Rao, *Phys. Rev. B*, 2006, **74**.
64. D. G. Wickham and J. B. Goodenough, *Phys Rev*, 1959, **115**, 1156-1158.
65. S. Blanco-Canosa, F. Rivadulla, V. Pardo, D. Baldomir, J. S. Zhou, M. Garcia-Hernandez, M. A. Lopez-Quintela, J. Rivas and J. B. Goodenough, *Phys. Rev. Lett.*, 2007, **99**.
66. D. Tobia, J. Milano, M. T. Causa and E. L. Winkler, *J. Phys.-Condes. Matter*, 2015, **27**.
67. I. S. Jacobs, *J. Phys. Chem. Solids*, 1960, **15**, 54.
68. A. N. Goryaga, L. G. Antoshina, A. I. Kokorev and D. A. Chursin, *Phys. Solid State*, 2002, **44**, 759.

RSC Advances Accepted Manuscript